Rare Metal Materials and Engineering
Volume 49, Issue 9, September 2020
Available online at www.rmme.ac.cn

Science Press

Cite this article as: Rare Metal Materials and Engineering, 2020, 49(9): 2913-2919.

ARTICLE

Parametric Investigation on Ti6Al4V Single Beads Produced by Electron Beam Freeform Fabrication: Geometry, Microstructure, Composition and Hardness

Tao Xuewei[1], Yao Zhengjun[1,2], Zhang Shasha[1,2]

[1] School of Materials Science and Technology, Nanjing University of Aeronautics and Astronautics, Nanjing 210016, China; [2] Key Laboratory of Materials Preparation and Protection for Harsh Environment of Ministry of Industry and Information Technology, Nanjing University of Aeronautics and Astronautics, Nanjing 210016, China

Abstract: Ti6Al4V single beads were prepared by electron beam freeform fabrication (EBF^3) to investigate the influence of wire-feed rate, beam power and travel speed on their geometry, microstructure, composition and the resulting hardness. Results show that an increased wire-feed rate favors to increase the deposition efficiency and geometry accuracy, but it requires affordable heat input to successfully deposit. The narrowed columnar β grains with the fine microstructural features inside and the decreased Al evaporation loss are available at an increased wire-feed rate/travel speed or a decreased beam power, which is attributed to the decreased temperature and dimension of molten pool. Therefore, the beads produced under such process parameters possess the increased hardness. This investigation reveals the correlation between the process parameters and structure and performance of deposited beads, which offers a valuable guidance for accurate manufacturing of multi-layered components with reliable microstructure and mechanical properties.

Key words: EBF^3; geometry; microstructure; Al loss; hardness

Electron beam freeform fabrication is a promising technology that has been developed for additive manufacturing (AM) and repairing of the large-scale metal components [1-3]. It is featured with high deposition rate, high density, reduced contamination and desirable material quality [3-5]. In general, the investigation on single beads is the first step towards attaining a desirable EBF^3-ed component. Single beads represent the fundamental unit for producing AM-ed components, and their geometry and solidified microstructure are the key characteristics to obtain the accurate molding shape and the reasonable mechanical properties [5,6]. Furthermore, the single beads can offer the validated results for simulation of AM process [6,7], and provide the guidance for closed-loop process control [7].

Ti6Al4V alloy is the most favorable material for direct metal AM processes. It has been widely applied in the aerospace and marine industries, owing to its high specific strength, good elevated-temperature mechanical property and excellent corrosion resistance [5-8]. In regard to the investigation on AM-ed Ti6Al4V single beads, Brandl et al [7,8] demonstrated that the geometry and microstructure of single beads are greatly dependent on the thermal history underwent, which is determined by the process parameters. It also reveals that the beam power and travel speed are the vital factors for the width and height of the single bead, respectively [9]. For the EBF^3 process, Gockel et al [6] found that the width of solidified prior β grains in single beads is proportional to the width of molten pool. The simulation results also reveal that a large dimensional molten pool is available at a high beam power or a low travel speed [10]. However, the research on the wire-feed rate is lacking. Additionally, the relationship between the solidified

Received date: September 11, 2019
Foundation item: National Natural Science Foundation of China (51975286); Postgraduate Research & Practice Innovation Program of Jiangsu Province (KYCX18_0272); Opening Project of Jiangsu Key Laboratory of Advanced Metallic Materials; Priority Academic Program Development of Jiangsu Higher Education Institution
Corresponding author: Yao Zhengjun, Ph. D., Professor, School of Materials Science and Technology, Nanjing University of Aeronautics and Astronautics, Nanjing 210016, P. R. China, Tel: 0086-25-84891921, E-mail: yaozj1921@126.com

microstructure and mechanical property is still ambiguous under the conditions of high deposition rates.

This work gives a comprehensive investigation on the geometry, microstructure and chemical composition of EBF^3-ed single beads in terms of the wire-feed rate, beam power and travel speed, and the resulting hardness was also studied.

1 Experiment

Single beads were produced from the Ti6Al4V wire with 1.6 mm in diameter via a laboratory EBF^3 machine equipped with a power source with 8 kW electron beam. The experiment was performed in the vacuum environment below 10^{-2} Pa. A schematic drawing of the deposition process is shown in Fig.1a. Detailed process parameters in terms of power (P), travel speed (v) and wire-feed rate (v_w) are given in Table 1, and the deposited single beads are presented in Fig.1b.

Three cross-sectional samples were extracted from the deposited beads. Prior to microstructural observation, the polished samples were etched with Kroll's reagent ($HF:HNO_3:H_2O$=4 mL:6 mL:90 mL). The stereomicroscope (SZN71) and optical microscope (BX53) were used to analyze the macro- and micro- structure, respectively. The geometric sizes of single beads were measured for the cross-sectional samples by Image-Pro Plus 6.0 software, including the width (W), height (H_a), area (A) and angle (θ) of additive material, height of remelted zone (H_r) and height of heat affected zone (H_{HAZ}), as shown in Fig.1c. The composition of element Al was detected by inductively-coupled plasma spectrometer (ICP) to evaluate the element loss. The hardness test was carried out on a micro-hardness tester (FM-700) at 500 g for 10 s.

2 Results and Discussion

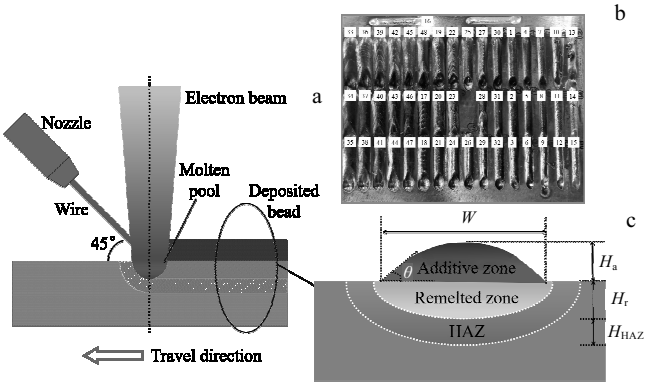

Fig.1 Schematic diagram of preparation (a); overview of deposited beads (b); schematic diagram of cross section for geometry measurement (c)

2.1 Geometric characteristics

The cross sections of deposited beads are presented in Fig.2. Differences in geometric characteristics of beads are visible, and the measured results are listed in Table 1. The width (W), height (H_a), area (A) and angle (θ) of additive materials against wire-feed rate are plotted in Fig.3. It can be seen that the W, H_a, A and θ of beads increase with increasing the wire-feed rate. A larger deposition amount of wire is achievable at a higher wire-feed rate, and therefore, the deposited area (A) increases. In this case, more molten deposit will spread itself in width and height, resulting in the increase of the W and H_a. However, the geometric sizes decrease rather than increase at a high wire-feed rate of 2000 mm/min with a low beam power (e.g. P4, P8, P12, P16) or a high travel speed (e.g. P28, P32). It is a result of mismatch between the heat input and wire-feed rate. When the wire feed is overspeed, the wire cannot be melted completely by a low heat input (i.e. low beam power and/or high travel speed) [9]. As a result, the wire tends to escape from the molten pool, leading to less deposition. In

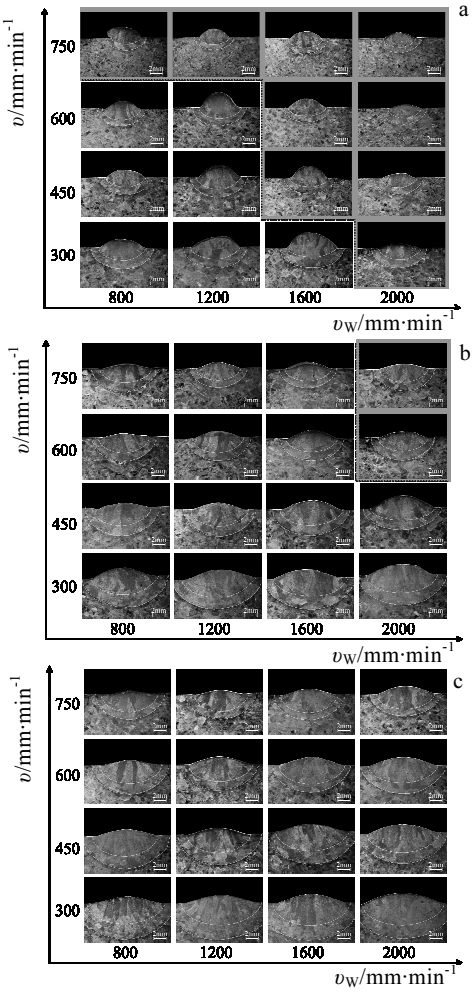

Fig.2 Cross sections of deposited beads at beam power of 1.8 kW (a), 3.0 kW (b) and 4.2 kW (c)

Table 1 Single bead matrix of the process and corresponding measured results

Parameter	P/kW	v/mm·min^{-1}	v_W/mm·min^{-1}	W/mm	H_a/mm	A/mm^2	θ/(°)	H_r/mm	H_{HAZ}/mm	D_β/μm	$HV_{0.5}$/MPa
1	1.8	300	800	7.51	1.43	7.24	33.24	1.98	1.35	507.1	3192
2	1.8	300	1200	7.88	1.80	9.78	40.25	1.94	1.34	482.2	3205
3	1.8	300	1600	8.12	2.55	12.54	51.45	1.65	1.33	455.8	3221
4	1.8	300	2000	6.46	0.74	3.24	22.76	—	—	—	—
5	1.8	450	800	6.36	1.21	5.68	36.45	1.73	1.14	408.9	3303
6	1.8	450	1200	6.89	2.38	8.95	47.38	1.97	1.10	390.7	3313
7	1.8	450	1600	6.55	1.82	8.54	43.90	—	—	—	—
8	1.8	450	2000	5.41	0.73	2.84	24.40	—	—	—	—
9	1.8	600	800	5.78	1.35	4.92	34.30	1.34	0.96	345.1	3375
10	1.8	600	1200	6.21	2.45	10.01	53.03	1.71	0.94	333.5	3391
11	1.8	600	1600	6.06	1.39	6.14	37.60	—	—	—	—
12	1.8	600	2000	5.17	0.79	2.21	23.75	—	—	—	—
13	1.8	750	800	5.25	1.53	7.57	47.65	—	—	—	—
14	1.8	750	1200	5.13	1.18	4.28	40.99	—	—	—	—
15	1.8	750	1600	5.19	1.23	4.69	45.20	—	—	—	—
16	1.8	750	2000	5.12	0.97	3.12	30.99	—	—	—	—
17	3.0	300	800	9.79	1.52	8.44	20.17	2.99	1.88	550.5	3106
18	3.0	300	1200	10.60	1.42	9.58	18.16	2.87	1.88	536.7	3121
19	3.0	300	1600	10.99	1.62	10.86	20.58	2.79	1.78	518.4	3140
20	3.0	300	2000	11.31	1.94	13.17	24.13	2.82	1.77	509.7	3156
21	3.0	450	800	8.10	0.93	5.54	15.44	2.79	1.52	520.6	3185
22	3.0	450	1200	8.63	1.18	7.01	20.55	2.55	1.51	507.9	3213
23	3.0	450	1600	9.56	1.50	9.68	22.86	2.40	1.49	482.5	3237
24	3.0	450	2000	10.49	1.99	13.16	26.39	1.81	1.47	449.6	3251
25	3.0	600	800	7.32	0.71	3.72	14.25	2.55	1.28	491.8	3272
26	3.0	600	1200	7.56	1.12	5.67	19.21	2.44	1.25	476.2	3274
27	3.0	600	1600	7.74	1.38	7.07	23.91	2.32	1.23	457.6	3291
28	3.0	600	2000	7.44	1.24	5.37	22.55	—	—	—	—
29	3.0	750	800	7.26	0.75	4.05	15.79	2.10	1.28	413.7	3289
30	3.0	750	1200	7.21	1.01	4.66	21.45	2.00	1.08	397.1	3338
31	3.0	750	1600	7.31	1.19	5.07	24.88	1.92	0.98	373.3	3365
32	3.0	750	2000	7.56	0.93	4.21	19.42	—	—	—	—
33	4.2	300	800	10.97	1.19	7.58	13.35	3.54	2.38	585.7	3070
34	4.2	300	1200	11.34	1.25	9.29	14.11	3.52	2.34	571.4	3101
35	4.2	300	1600	11.48	1.39	11.19	15.66	3.56	2.31	558.3	3146
36	4.2	300	2000	13.21	1.58	14.43	16.05	3.42	2.27	540.1	3152
37	4.2	450	800	9.13	1.02	5.56	16.35	3.18	1.94	552.4	3139
38	4.2	450	1200	9.80	1.13	7.38	17.25	3.14	1.85	533.8	3166
39	4.2	450	1600	10.45	1.21	9.47	18.23	3.06	1.81	519.7	3188
40	4.2	450	2000	10.80	1.43	11.59	20.38	3.05	1.73	506.6	3196
41	4.2	600	800	9.38	0.85	4.31	11.65	2.91	1.58	523.2	3187
42	4.2	600	1200	9.82	1.21	7.04	16.35	2.75	1.40	503.8	3193
43	4.2	600	1600	10.25	1.29	8.74	17.13	2.85	1.48	490.8	3199
44	4.2	600	2000	10.77	1.38	10.08	18.81	2.82	1.45	473.1	3216
45	4.2	750	800	7.43	0.59	3.44	10.51	2.91	1.20	497.1	3135
46	4.2	750	1200	7.49	0.69	4.47	13.45	2.79	1.14	472.2	3159
47	4.2	750	1600	8.02	0.95	5.01	16.23	2.75	1.11	461.4	3142
48	4.2	750	2000	9.34	1.32	7.95	19.67	2.40	1.10	431.2	3197

particular, this phenomenon prefers to occur at a low heat input, even if the wire-feed rate is low. After evaluating, the mismatched process parameters include P4, P7, P8, P11~P16, P28 and P32, which will not be discussed in the follows.

A further experimental finding is that the wire-feed rate has a greater effect on the H_a than on the W at low beam powers, whereas the effect of wire-feed rate on the H_a and W is inverse under the high beam power conditions. A feasible explanation is that the molten metal produced by a low beam power has a low fluidity, favoring the increase in the height rather than in the width [8]. However, its fluidity increases with the increase of beam power due to the increased temperature, and thus, the gravity effect gradually dominates rather than the surface tension [11]. Consequently, more molten metal will flow toward the sides, which results in a greater increase in the W.

It is also observed that the W of the beads increases with increasing the beam power, while the H_a and θ decrease when the travel speed and wire-feed rate are constant. The A is not significantly influenced due to the constant deposition amount of wire. As aforementioned, the fluidity of molten metal increases at a high beam power, resulting in the increase of the W, and meanwhile its H_a and θ decrease. As the travel speed increases, the W, H_a and A decrease. On one hand, low temperature of molten metal induced by an

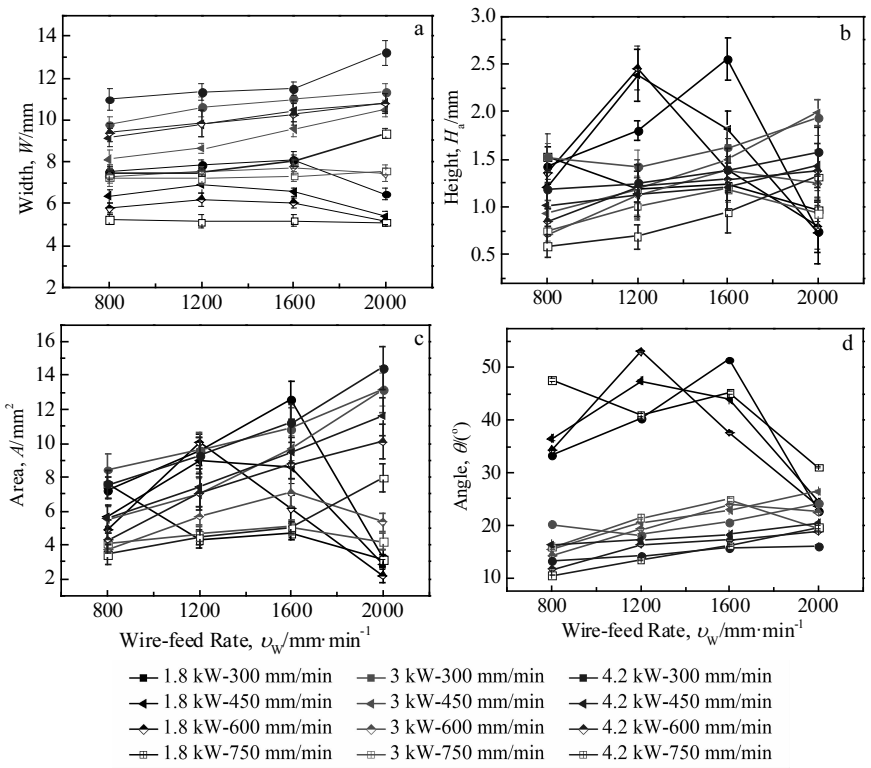

Fig.3 Width (a), height (b), area (c) and angle (d) of additive material as a function of wire-feed rate

increased travel speed leads to the decrease of its fluidity, and therefore, the W decreases. On the other hand, the actual deposition amount of wire decreases with increasing the travel speed, as the wire-feed rate is constant [8], and consequently, the A, W and H_a of beads decrease.

Fig.4 reveals that the height of the remelted zone (H_r) and HAZ (H_{HAZ}) decrease with increasing the wire-feed rate and travel speed, whereas they increase with increasing the beam power. It has been demonstrated that the H_r and H_{HAZ} are proportional to the dimension of molten pool [8]. According to Ref.[12], a high deposition efficiency is available at an increased beam power or a decreased wire-feed rate, which indicates that the excess heat is absorbed by the molten pool. As a result, the temperature of molten pool increases, and its dimension enlarges, and thus, the H_r and H_{HAZ} increase. At a constant beam power and wire-feed rate, an increased travel speed decreases the temperature of molten pool and its dimension due to the increased thermal gradient and cooling rate [8,12], which results in the decrease of H_r and H_{HAZ}.

2.2 Solidified morphology and microstructure

Columnar prior β-grains that grow from the remelted

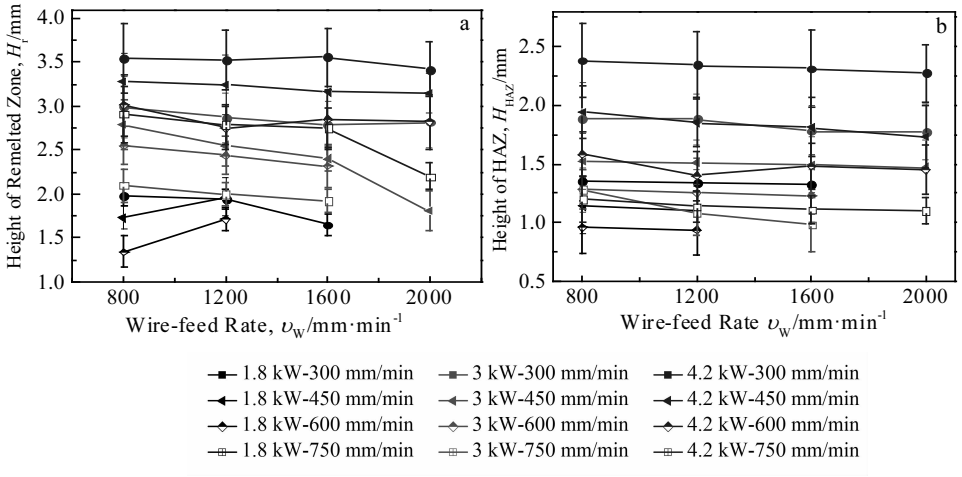

Fig.4 Height of the remelted zone (a) and HAZ (b) as a function of wire-feed rate

zone to additive zone are visible in the deposited beads, as shown in Fig.5. The columnar morphology is the result of the epitaxial growth of prior β-grains during solidification due to the maximum temperature gradient [13,14]. The average width (D_β) of columnar β-grains is measured using the linear intercept method, and the results are summarized in Table 1.

The D_β against the wire-feed rate is plotted in Fig.6. It is obvious that the D_β decreases with increasing the wire-feed rate (e.g. D_β=585.7 μm for P33 and D_β=540.1 μm for P36, as shown in Fig.5). Less heat is absorbed into the molten pool when the wire-feed rate is high, resulting in a decreased temperature of molten pool. It facilitates the increase of cooling rate [8], and consequently, the D_β in the beads at an increased wire-feed rate is fine. On the contrary, a large D_β is obtained at a high beam power or a low travel speed, due to the decreased cooling rate induced by hotter molten pool under such process conditions.

The OM and SEM images of Fig.7 and Fig.8 illustrate that the individual columnar β-grains in beads are composed of a basket-weave structure and a few martensitic α. In addition, the interlamellar spacing of α lath is 0.78 μm at P33 (Fig.8a), while that is 0.65 μm at P36 (Fig.8b), indicating that α lath in basket-weave structure appears to be fine as the wire-feed rate increases. Differences in the microstructural features are primarily dependent on the cooling rate undergone during the transition of $\beta \rightarrow \alpha$. Generally, the fine spacing of α lath is available at high cooling rates due to the large undercooling [14]. An increased wire-feed rate induces a decrease in temperature of molten pool, favoring a high cooling rate [7,8], and therefore, the fine basket-weave structure develops. The observations are consistent with the investigation on aluminum alloy produced by EBF^3 [12].

2.3 Chemical composition

The evaporation of Al element occurs inevitably during the electron beam deposition of Ti6Al4V alloys due to its great volatility [1,15]. The content of Al element in wire, base plate and partial deposited beads is measured, as listed in Table 2. Indeed, the Al element

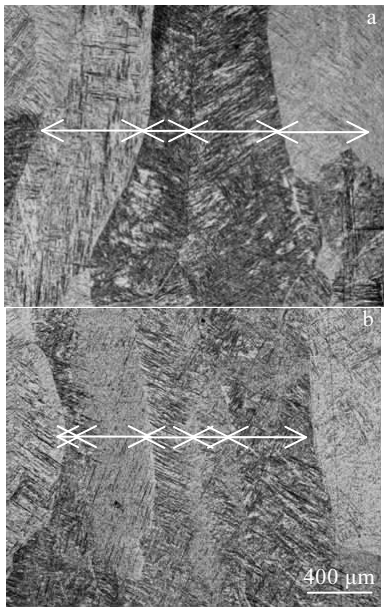

Fig.5 Columnar β-grains in single beads produced under parameters P33 (a) and P36 (b) (arrows indicate width of columnar prior β-grains)

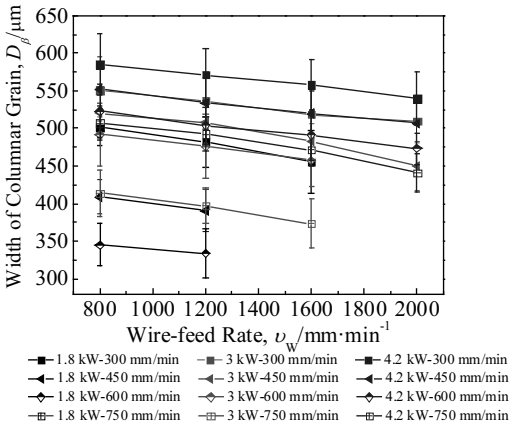

Fig.6 Width of columnar β-grains as a function of wire-feed rate

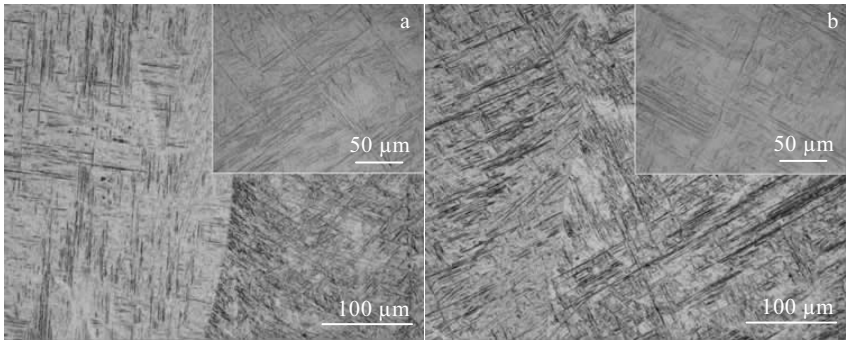

Fig.7 OM images of typical microstructure in beads under parameters P33 (a) and P36 (b)

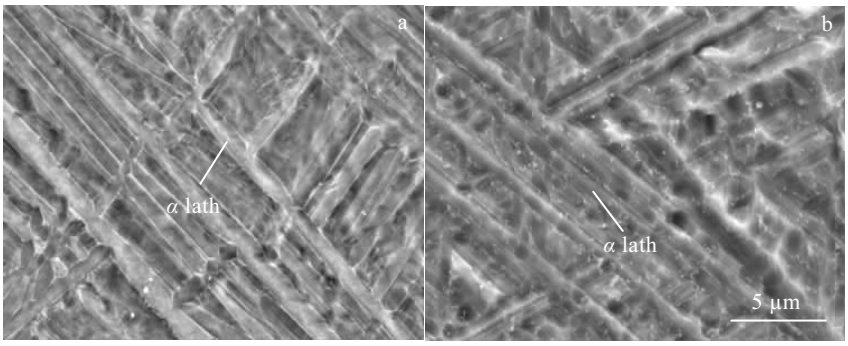

Fig.8 SEM images of basket-weave structure in beads under parameter P33 (a) and P36 (b)

Table 2 Content of Al element in wire, base plate and partial deposited beads

Parameter	Al content/wt%	Al loss/%
Wire	6.05	—
Base plate	6.12	—
P1	5.14	15.02
P3	5.51	8.91
P17	5.06	16.34
P20	5.40	10.74
P29	5.20	14.05
P31	5.57	7.92
P33	4.94	18.34
P36	5.29	12.56
P45	5.11	15.51
P48	5.48	9.41

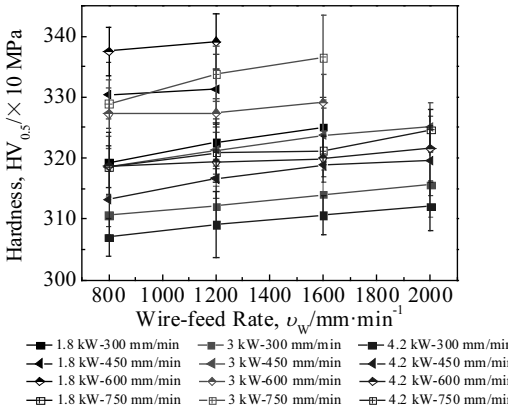

Fig.9 Hardness of the additive zone as a function of wire-feed rate

evaporation is observed in all tested single beads. At a constant beam powers, the Al loss at a decreased wire-feed rate is less than at an increased wire-feed rate. It indicates that the wire-feed rate plays an important role in the evaporation of Al element, and the increased wire-feed rate yields the Al loss. The increased travel speed has the similar effect, whereas an increased beam power strongly accelerates the Al loss. The finding is consistent with other investigation [15,16]. It has been demonstrated that the evaporation of Al element is related to the temperature and surface area-to-volume ratio of molten pool, and both high temperatures and high surface area-to-volume ratios facilitate the Al evaporation [1,16]. As the wire-feed rate/travel speed increases or the beam power decreases, heat absorption in the molten pool is reduced, and thus, its temperature and dimension decrease, leading to the restricted Al loss. In a word, under the condition of complete melting of wire, the Al loss can be minimized by the increase in wire-feed rate/travel speed and the decrease in beam power during the EBF^3 of Ti6Al4V alloys.

2.4 Hardness

The hardness of deposited beads is measured and given in Table 1. Fig.9 shows the variation in hardness with the wire-feed rate. It is observed that the hardness increases with increasing the wire-feed rate. Furthermore, the hardness increases with increasing the travel speed, while it decreases with increasing the beam power. Generally, the deposited beads can be hardened by boundary hardening, dislocation and solid solution hardening[7,13]. As aforementioned, the fine basket-weave structure and the decreased Al loss are achievable at a high wire-feed rate/travel speed or a low beam power. The fine microstructural feathers (e.g. fine α lath) provide more boundaries and/or dislocations, which results in the enhanced hardness [7,13]. Additionally, the decreased Al loss increases the solid solution hardening of Al element, and the loss of hardness is reduced. As a result, the bead at an increased wire-feed rate possesses a high hardness, as well as at an increased travel speed and a decreased beam power.

3 Conclusions

1) A large amount of heat input by decreasing wire-feed rate/travel speed or increasing beam power can increase the affordability of deposition, while the fluidity and gravity effect of molten metal increases, leading to a decrease in

geometry accuracy of beads.

2) As the wire-feed rate/travel speed increases or the beam power decreases, both the columnar β grains and the microstructural feature inside appear to be fine, ascribed to the increased cooling rate.

3) The Al evaporation loss can be minimized by the increase in wire-feed rate/travel speed or the decrease in beam power, due to the decrease in temperature and dimension of molten pool.

4) The fine basket-weave structure and the decreased Al loss play a certain role in the increase of hardness, which can be achieved at an increased wire-feed rate/travel speed or a decreased beam power.

References

1 DebRoy T, Wei H, Zuback J *et al*. *Progress in Materials Science*[J], 2018, 92: 112

2 Suo H B, Chen Z Y, Liu J R *et al*. *Rare Metal Materials and Engineering* [J], 2014, 43(4): 780

3 Liu Z, Zhao Z B, Liu J R *et al*. *Material Science and Engineering A*[J], 2019, 742: 508

4 Tao X W, Yao Z J, Zhang S S *et al*. *JOM*[J], 2019, 71(7): 2313

5 Hayes B J, Martin B W, Welk B *et al*. *Acta Materialia*[J], 2017, 138: 120

6 Gockel J, Beuth J, Taminger K. *Additive Manufacturing*[J], 2014, 1-4: 119

7 Brandl E, Michailov V, Viehweger B *et al*. *Surface & Coating Technology*[J], 2011, 206: 1120

8 Brandl E, Michailov V, Viehweger B *et al*. *Surface & Coating Technology*[J], 2011, 206: 1130

9 Mok S H, Bi G, Folkes J *et al*. *Surface & Coating Technology*[J], 2008, 202: 3933

10 Soylemez E, Beuth J, Taminger K. *Proceeding 21th International Solid Freeform Fabrication Symposium*[C]. Austin: SFF, 2010: 571

11 Taminger K, Harley R. *Proceeding 13th International Solid Freeform Fabrication Symposium*[C]. Austin: SFF, 2002: 482

12 Sankaran S, Taminger K, Hafley R *et al*. *Aero Mat 2008 Conference and Exposition* [C]. Austin: ASM International, 2008

13 Brandl E, Schoberth A, Leyens C. *Materials Science and Engineering A*[J], 2012, 532: 295

14 Vrancken B, Thijs L, Kruth J P *et al*. *Journal of Alloys and Compounds*[J], 2012, 541: 177

15 Juechter V, Scharowsky T, Singer R *et al*. *Acta Materialia*[J], 2014, 76: 252

16 Brice C, Rosenberger B, Sankaran S *et al*. *Materials Science Forum*[J], 2009, 618-619: 155

电子束熔丝成形 Ti6Al4V 单道沉积体的工艺研究：几何尺寸、显微组织，成分及硬度

陶学伟[1]，姚正军[1,2]，张莎莎[1,2]

(1. 南京航空航天大学 材料科学与技术学院，江苏 南京 210016)

(2. 南京航空航天大学 面向苛刻环境的材料制备与防护技术工信部重点实验室，江苏 南京 210016)

摘　要：采用电子束熔丝成形工艺制备了 Ti6Al4V 单道沉积体，并研究了送丝速度、束流功率和行进速度等工艺参数下沉积体的几何尺寸、显微结构、成分以及硬度的变化。结果表明，加快送丝速度有利于提高沉积效率及成形精度，但需要足够的热输入以保证沉积顺利。当送丝速率、行进速度增大或束流功率减小时，由于熔池温度和尺寸的减小，可以获得较窄的柱状 β 晶及其内部细小的组织特征，同时铝蒸发损耗降低。因此，采用这些工艺制备的沉积体具有更高的硬度。本研究揭示了工艺参数与沉积体结构性能之间的关系，为制造具有可靠组织结构和力学性能的多层构件提供有价值的指导。

关键词：电子束熔丝沉积；几何尺寸；显微组织；Al损耗；硬度

作者简介：陶学伟，男，1989 年生，博士生，南京航空航天大学材料科学与技术学院，江苏 南京 210016，电话：025-84891921，E-mail: tao_xuewei@126.com